

Optical evidence for a spin-filter effect in the charge transport of $Eu_{0.6}Ca_{0.4}B_6$

A. Perucchi, G. Caimi and H.R. Ott

Laboratorium für Festkörperphysik, ETH Zürich, CH-8093 Zürich, Switzerland

L. Degiorgi

*Paul Scherrer Institute, CH-5232 Villigen and Laboratorium für Festkörperphysik,
ETH Zürich, CH-8093 Zürich, Switzerland*

A.D. Bianchi and Z. Fisk

NHMFL-FSU, Tallahassee FL 32306, U.S.A.

(Dated: June 11, 2018)

Abstract

We have measured the optical reflectivity $R(\omega)$ of $Eu_{0.6}Ca_{0.4}B_6$ as a function of temperature between 1.5 and 300 K and in external magnetic fields up to 7 T. The slope at the onset of the plasma edge feature in $R(\omega)$ increases with decreasing temperature and increasing field but the plasma edge itself does not exhibit the remarkable blue shift that is observed in the binary compound EuB_6 . The analysis of the magnetic field dependence of the low temperature optical conductivity spectrum confirms the previously observed exponential decrease of the electrical resistivity upon increasing, field-induced bulk magnetization at constant temperature. In addition, the individual exponential magnetization dependences of the plasma frequency and scattering rate are extracted from the optical data.

PACS numbers: 78.20.Ls, 75.50.Cc

Remarkable variations of electronic transport properties, distinctly depending on the bulk magnetization, have been observed for materials, such as rare-earth hexaborides and manganites^{1,2}. A very direct link between electronic transport and bulk magnetization M was revealed by measurements of magneto-optical properties of ferromagnetic EuB_6 (Refs. 3 and 4), exhibiting a substantial blue shift of the plasma edge in the optical reflectivity with decreasing temperature and increasing magnetic field H (Refs. 5 and 6).

More recently, dc magneto-transport and magnetization experiments on a series of $Eu_{1-x}Ca_xB_6$ compounds provided results that again reflect the intimate relation between the electronic conductivity and the magnetization. In particular, for material with $x=0.4$, an exponential decrease of the resistivity ρ_{dc} as a function of magnetization at constant temperature close to and below the Curie temperature T_C was reported⁷. Based on these results it was suggested that some kind of magnetization-dependent barriers or intrinsic spin-filter effects dominate the electronic transport in the magnetically ordered phase of this material⁷.

It therefore seemed of interest to further characterize the charge transport in *Ca*-doped EuB_6 by investigating the electrodynamic response. Since $\rho_{dc} \sim \Gamma/\omega_p^2$, where Γ and ω_p are the scattering rate and the plasma frequency of the itinerant charge carriers, respectively, it is instructive to single out the relevance of those quantities in relation with the dc properties. The measured optical response and its phenomenological analysis, based on the classical dispersion theory, offers this possibility and provides information on important electronic parameters, including the disorder-induced scattering rate of the charge carriers.

The single-crystal of $Eu_{0.6}Ca_{0.4}B_6$ was prepared by solution growth from *Al* flux, using the necessary high purity elements as starting materials. Our specimen ($1.7 \times 1.7 \times 0.5 \text{ mm}^3$) is from the same thoroughly characterized batch of samples described in Ref. 7. From the absence of any sharp features in $\rho_{dc}(T)$ at 1.2 K , the critical temperature for superconductivity of *Al*, we exclude the presence of *Al* inclusions in the sample⁷. The optical reflectivity $R(\omega)$ was measured in a broad spectral range from the far infrared to the ultraviolet and as a function of both temperature and magnetic field. The corresponding experimental details are described in Refs. 5 and 6.

Figure 1 summarizes the relevant reflectivity $R(\omega)$ results, at selected temperatures from above to below T_C and as a function of the external magnetic field. We limit our presentation to the spectral range from the far infrared (FIR) up to the mid-infrared, where the field and temperature induced variations of $R(\omega)$ are most prominent. Around 5000 cm^{-1} all recorded

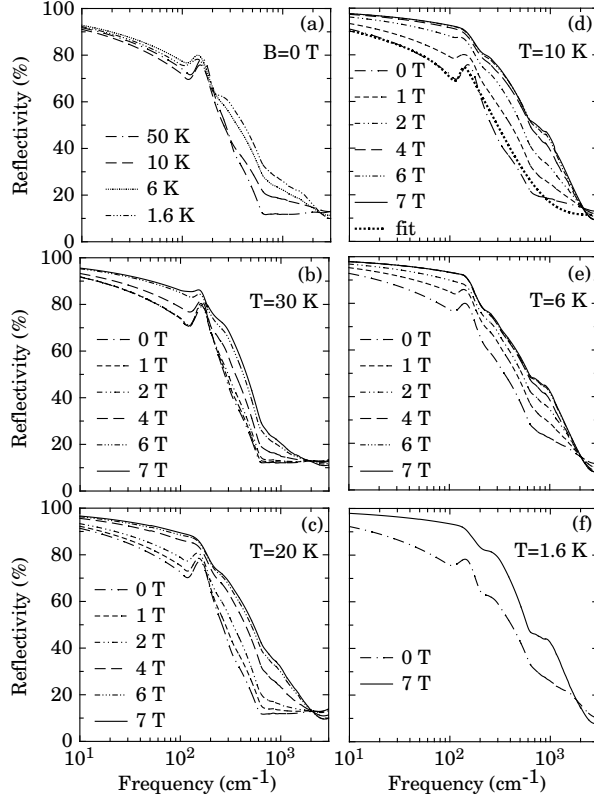


FIG. 1: (a) Optical reflectivity $R(\omega)$ of $Eu_{0.6}Ca_{0.4}B_6$ in zero field at temperatures between 50 and 1.6 K. (b)-(f) Magnetic field dependence of $R(\omega)$ at selected temperatures. In panel (d) the Lorentz-Drude phenomenological fit at 10 K and 0 T is also reproduced in order to demonstrate the fit quality.

$R(\omega)$ spectra merge and above 50 K no field dependence is observed. A comparison with previously published data for EuB_6 (Ref. 6) reveals distinct differences. Although the reflectivity is still of metallic type, the onset of its plasma edge in zero field is broad in Ca -doped EuB_6 , i.e., a much less sharp feature than the increase of $R(\omega)$ with decreasing ω for EuB_6 . Another difference is the much less pronounced blue shift of the plasma edge with decreasing temperature or increasing field in the Ca -doped material in comparison with the features of the binary compound⁶. The peak at about 150 cm^{-1} is an optically active phonon⁵. A closer inspection of the data reveals a small shift of this phonon mode to lower frequencies at temperatures below 6 K. The other infrared active phonon, observed around 850 cm^{-1} in EuB_6 (Refs. 5 and 6), can barely be identified here. It appears as a tiny spike, almost completely screened by the plasma edge. Since it is of no relevance in

this work, we do not discuss it further. At fixed temperature but increasing magnetic field, the reflectivity is, overall, progressively enhanced, thus screening the phonon mode at 150 cm^{-1} . The $R(\omega)$ enhancement results mostly from an increasing slope of the plasma edge feature with increasing field. With decreasing temperature and increasing field we note the appearance of a pronounced shoulder at about 1000 cm^{-1} , overlapping the plasma edge. We also remark that the behaviour of $R(\omega)$ in zero field (Fig. 1a) and decreasing temperature is qualitatively similar to $R(\omega)$ at fixed temperature and increasing field, i.e., it steadily increases with decreasing temperature. Although not presented here, similar optical $R(\omega)$ results were obtained for other concentrations of *Ca*-doping (e.g., 10% and 20%).

Below 30 cm^{-1} , our lower experimental limit, the Hagen-Rubens (HR) extrapolation⁸ was used for the extension of $R(\omega)$ towards zero frequency. In the FIR spectral range the relative increase of $R(\omega)$ at fixed temperature but increasing magnetic field qualitatively agrees with the trend observed in the dc electronic transport data⁷, which exhibits a significant negative magnetoresistance below 50 K . Unexpected and puzzling is the temperature dependence of $R(\omega)$ in zero field, shown in Fig. 1a. At the lowest experimentally accessible frequency, $R(\omega)$ is consistent with the HR extrapolation using, however, σ_{dc} values that are not in agreement with those of Ref. 7. The σ_{dc} values used in the HR extrapolation increase instead of decreasing by a factor of four between 20 and 2 K . Inserting the σ_{dc} values of Ref. 7 would imply that $R(\omega)$ at low frequencies and in zero field decreases with decreasing temperature. This is not compatible with the experimental findings, at least above 30 cm^{-1} (Fig. 1a). Optical experiments in the microwave range, i.e. below 30 cm^{-1} , may eventually solve this puzzle and reconcile the optical results with the dc transport properties. Our interest here is focussed on the relative magnetic field dependence, which does not suffer from the inconsistencies between dc and dynamical properties. Therefore, we have not attempted to extrapolate the optical data in zero field by forcing an agreement with σ_{dc} of Ref. 7. As it will be clear below, our choice for σ_{dc} in zero field neither alters the main content of our discussion nor does it affect the conclusion of our work.

The Kramers-Kronig transformations⁸ of $R(\omega)$ allow us to extract the optical functions, such as the real part $\sigma_1(\omega)$ of the optical conductivity. As an example we show $\sigma_1(\omega)$ at 10 K and 7 T in Fig. 2. At low frequencies one can easily recognize the metallic component of $\sigma_1(\omega)$, where the limit $\sigma_1(\omega \rightarrow 0)$ reflects the dc conductivity⁹. Above 100 cm^{-1} and up to the mid-infrared, $\sigma_1(\omega)$ saturates to an almost constant value. Above 10^4 cm^{-1}

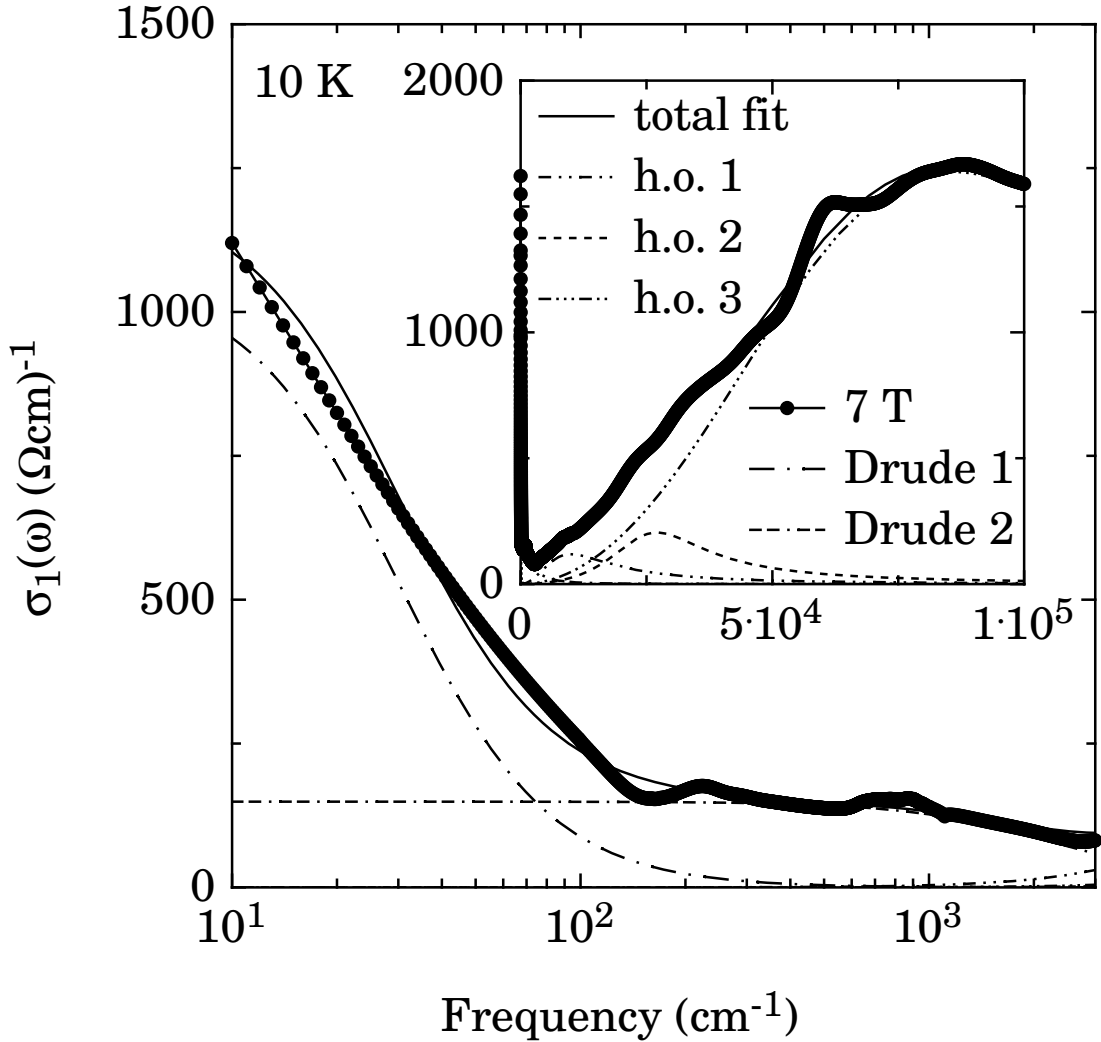


FIG. 2: Real part $\sigma_1(\omega)$ of the optical conductivity at 10 K and 7 T with the fit components. The main panel emphasizes the spectral range of the two Drude terms, while the inset displays the spectral range pertinent for the three harmonic oscillators (h.o.). The component of the phonon mode is not shown here. The parameters are (cm^{-1}): (Drude plasma frequencies) $\omega_p^{D1} = 1382$, $\omega_p^{D2} = 4633$; (Drude scattering rates) $\Gamma_1 = 30$, $\Gamma_2 = 2401$; (h.o. strengths) $\omega_{p1} = 11207$, $\omega_{p2} = 17070$, $\omega_{p3} = 111627$; (h.o. scattering rates) $\Gamma_{01} = 17635$, $\Gamma_{02} = 23717$, $\Gamma_{03} = 126874$; (h.o. resonance frequencies) $\omega_{01} = 9986$, $\omega_{02} = 27058$, $\omega_{03} = 85844$ (Ref. 10).

(inset of Fig. 2) we note the clear onset of interband transitions^{5,6}. The $R(\omega)$ and $\sigma_1(\omega)$ spectra, for any combination of temperature and magnetic field, can be well reproduced by employing the Lorentz-Drude model based on the classical dispersion theory^{6,8}. Figure 2

also displays the different components resulting from the fit. Apart from two temperature and field independent Lorentz harmonic oscillators (h.o. 2 and 3) in the frequency range above $1.6 \times 10^4 \text{ cm}^{-1}$ (2 eV), we consider a temperature and field dependent h.o. 1 at about 9900 cm^{-1} (1.2 eV). Also the phonon mode at 150 cm^{-1} was described with a h.o. In order to account for the optical properties in the far and mid-infrared spectral range (i.e., $\omega < 3000 \text{ cm}^{-1}$), two Drude resonances must be considered. For simplicity, we will call them first (D1) and second (D2) Drude term, respectively. The total spectral weight encountered in the metallic component of $\sigma_1(\omega)$, i.e., the sum of the squared plasma frequencies of the two Drude terms, defines the effective plasma frequency of $Eu_{0.6}Ca_{0.4}B_6$. The two-Drude terms suggest a scenario where two different types of charge carriers exist. Those charge carriers belong to two bands (e.g., a conduction and an impurity band), are differently affected by the ferromagnetic transition, i.e., are differently coupled to the spin system (see below), and are characterized by distinct scattering rates and effective masses.

We fit the optical properties by allowing for changes of the plasma frequency of both Drude terms (ω_p^{D1} and ω_p^{D2} , respectively), of the strength of the h.o. 1 (ω_{p1}) and the scattering rate (Γ_1) of the first Drude term¹⁰. The first Drude term is characterized by a rather small, temperature and field-dependent scattering rate (Γ_1). The second Drude component mainly accounts for the spectral weight background of $\sigma_1(\omega)$ causing the shoulder most prominently seen at 1000 cm^{-1} in $R(\omega)$ at low temperatures and high fields (Fig. 1). Its scattering rate (Γ_2) is large and does not vary with temperature and field. Upon decreasing temperature or increasing field, both Drude terms acquire spectral weight, which is transferred down from higher energies, i.e., from the h.o. 1. As a consequence of the increasing screening by the itinerant carriers, the phonon mode component disappears with increasing field or decreasing temperature.

Figure 3 captures the main results of this study. In panel (a) we plot $1/(\omega_p^{D1})^2$ as a function of M (Ref. 11), while panel (b) shows the scattering rate $\Gamma_1(M)$ of the first Drude term (Fig. 2). At all temperatures below 30 K, we find that these two quantities may be well described by

$$(\omega_p^{D1}(M))^{-2} = (\omega_{p0})^{-2} e^{-\beta_\omega M} \quad (1)$$

and

$$\Gamma_1(M) = \Gamma_0 e^{-\beta_\Gamma M}, \quad (2)$$

where ω_{p0} and Γ_0 as well as β_ω or β_Γ are constants whose values are listed in the caption of Fig. 3. From the Lorentz-Drude fit parameters we can calculate the conductivity at $\omega=0$ from $\sigma_1(\omega = 0) = \sigma_1^{Drude1}(\omega = 0) + \sigma_1^{Drude2}(\omega = 0) = \sigma_{dc}$, and $\rho_{dc} = 1/\sigma_{dc}$. Panel (c) shows the ρ_{dc} values, normalized by $\rho_{dc}(M = 0)$ at each temperature, as a function of M . On purpose we have chosen the same representation of $\rho_{dc}(M)/\rho_{dc}(M = 0)$ versus M as first suggested empirically in Ref. 7. The functional form of eq. (1) is the best possible choice to fit the Drude weight variation. The choice of $(\omega_p^{D1}(M))^2$ varying linearly with M (as for EuB_6 , Ref. 6) is obviously inadequate.

It may immediately be seen from Fig. 3c that the expression

$$\rho_{dc}(M)/\rho_{dc}(M = 0) = Ae^{-\beta M} \quad (3)$$

describes very nicely the ρ_{dc} values calculated from the Lorentz-Drude fit parameters at $\omega = 0$. It turns out that the best fit to the data points in panel (c) employing eq. (3), is very close to the product of eq. (1) and (2), such that $\beta \sim \beta_\omega + \beta_\Gamma$. Both β_Γ and β_ω are of equal magnitude, suggesting that eq. (1) and (2) are of equal importance in shaping the exponential behaviour of eq. (3). The difference in $\rho_{dc}(M)/\rho_{dc}(M = 0)$ for temperatures below 6 K and well above T_C , is mainly due to the differences of the corresponding scattering rates (Γ_1) (Fig. 3b). Therefore, the first Drude term is the most relevant component in determining the dc ($\omega \rightarrow 0$) transport properties and governs to a great extent the temperature and magnetic field dependence of $\sigma_1(\omega)$ at low frequencies. With respect to the dc properties, the contribution from the second Drude term is only of marginal relevance.

The two temperature regimes identified in Fig. 3c for temperatures below 6 K and well above T_C have been found in Ref. 7 as well, even though $\rho_{dc}(M)/\rho_{dc}(M = 0)$ was larger at 12 K than at 2 K (see Fig. 4 in Ref. 7). This is the consequence of using the $\rho_{dc}(M = 0)$ values for the normalized representation in Fig. 3c as they follow from the optical results. These, as stated above, do not track the measured dc transport data⁷.

Wigger *et al.* suggested that some intrinsic magnetization dependent spin-filter effect dictates the electronic conduction in this material. The exponential variation of $\rho_{dc}(M)$ (eq. (3)) was viewed as being due to magnetization dependent tunnel barriers, caused by the domain walls of the ferromagnetically ordered phase in zero external field, which limit the motion of electrons. The domain walls are thought to be favored by the disorder on the cation-sublattice and to be progressively weakened and removed upon increasing

magnetization⁷. This disorder is most likely also responsible for the rather broad onset of the plasma edge feature in $R(\omega)$, at least at high temperatures and low fields (Fig. 1). The results and the conclusions which follow from the analysis of the optical data (Fig. 3) confirm the results obtained in the previous investigation of dc magnetotransport properties⁷. In addition, however, they allow for an analysis of the individual magnetization dependences of the two quantities that determine the dc transport, i.e., the plasma frequency and the scattering rate. The exponential variations that link the magnetization to the Drude spectral weight, which is proportional to the ratio n/m of the charge carrier concentration (n) and the effective mass (m), and to the scattering rate, is rather intriguing. It remains to be seen how these findings can be explained on a microscopic level.

Acknowledgments

The authors wish to thank J. Mueller for technical help and G.A. Wigger and R. Monnier for fruitful discussions. This work has been supported by the Swiss National Foundation for the Scientific Research.

¹ H.R. Ott, J.L. Gavilano, B. Ambrosini, P. Vonlanthen, E. Felder, L. Degiorgi, D.P. Young, Z. Fisk and R. Zysler, *Physica B* **281-282**, 423 (2000), and References therein.

² S. Jin, T.H. Tiefel, M. McCormack, R.A. Fastnacht, R. Ramesh and L.H. Chen, *Science* **264**, 413 (1994).

³ C.N. Guy, S. v. Molnar, J. Etourneau and Z. Fisk, *Solid State Commun.* **33**, 1055 (1980).

⁴ S. Paschen, D. Pushin, M. Schlatter, P. Vonlanthen, H.R. Ott, D.P. Young and Z. Fisk, *Phys. Rev. B* **61**, 4174 (2000).

⁵ L. Degiorgi, E. Felder, H.R. Ott, J.L. Sarrao and Z. Fisk, *Phys. Rev. Lett.* **79**, 5134 (1997).

⁶ S. Broderick, B. Ruzicka, L. Degiorgi, H.R. Ott, J.L. Sarrao and Z. Fisk, *Phys. Rev. B* **65**, 121102(R) (2002).

⁷ G.A. Wigger, Ch. Wälti, H.R. Ott, A.D. Bianchi and Z. Fisk, *Phys. Rev. B* **66**, 212410 (2002).

⁸ F. Wooten, in "Optical Properties of Solids", (Academic Press, New York, 1972), and M. Dressel and G. Grüner, in "Electrodynamics of Solids", (Cambridge University Press, 2002).

⁹ Although not shown explicitly, we note that the low frequency part ($\omega < 100 \text{ cm}^{-1}$) of $\sigma_1(\omega)$ narrows with decreasing temperature and increasing field. This is the consequence of the enhanced $R(\omega)$ at low frequencies with increasing field and decreasing temperature (Fig. 1).

¹⁰ The complete set of fit parameters for all measured combinations of field and temperature can be found at the link: <http://www.solidphys.ethz.ch/spectro/suppinfo/EuCaB6-MOR.pdf>

¹¹ The magnetization has been measured up to 5.5 T (Ref. 7). By assuming a Brillouin function for the overall behaviour of $M(H, T)$, a simple fit of the measured magnetization data leads to the values of M at 6 and 7 T for different temperatures (We specially thank G.A. Wigger for performing these fits). These extrapolated values were then combined with the corresponding optical parameters (ω_p and Γ), obtained from the optical spectra up to 7 T.

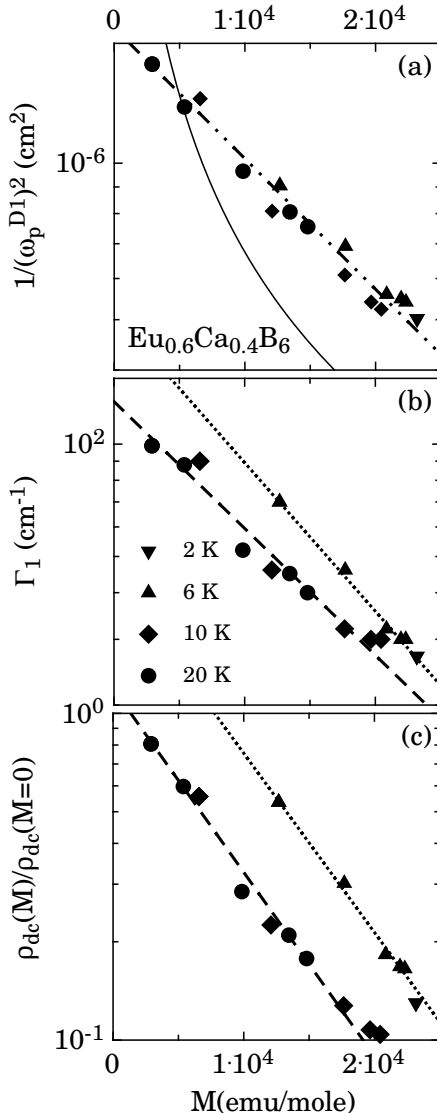


FIG. 3: Inverse squared plasma frequency $1/(\omega_p^{D1})^2$ of the first Drude term as a function of the magnetization M . The dash-dot-dot line represents eq. (1) with the parameters $\omega_{p0}=744$ cm $^{-1}$ and $\beta_\omega=5.75 \times 10^{-5}$ (emu/mole) $^{-1}$. The inadequate fit with $(\omega_p^{D1}(M))^2 \sim M$ (as for EuB_6 , Ref. 6) is also shown as thin solid line. (b) Scattering rate Γ_1 of the first Drude term as a function of M . The dotted and the dashed lines represent eq. (2) with the parameters $\Gamma_0 = 224$ cm $^{-1}$ and $\beta_\Gamma = 9.16 \times 10^{-5}$ (emu/mole) $^{-1}$ for 2 and 6 K, and $\Gamma_0 = 130$ cm $^{-1}$ and $\beta_\Gamma = 7.82 \times 10^{-5}$ (emu/mole) $^{-1}$ for 10 and 20 K, respectively. (c) $\rho_{dc}(M)/\rho_{dc}(M=0)$ versus M , calculated from the Lorentz-Drude fit parameters as described in the text. The dashed and the dotted lines are calculations based on eq. (3) with parameters $A = 1.19$ and $\beta = 1.30 \times 10^{-4}$ (emu/mole) $^{-1}$ for 10 and 20 K, and $A = 2.67$ and $\beta = 1.26 \times 10^{-4}$ (emu/mole) $^{-1}$ for 2 and 6 K, respectively. It is obvious that $\beta \sim \beta_\Gamma + \beta_\omega$ (see text).